



**An electrochemical platform for localized pH control on demand**

Journal:	<i>Lab on a Chip</i>
Manuscript ID	LC-ART-03-2016-000421.R2
Article Type:	Paper
Date Submitted by the Author:	09-May-2016
Complete List of Authors:	Fomina, Nadezda; Robert Bosch LLC, Corporate Research Johnson, Christopher; Robert Bosch LLC, Corporate Research Maruniak, Autumn; Robert Bosch LLC, Corporate Research Bahrampour, Soheil; Robert Bosch LLC, Corporate Research Lang, Christoph; Robert Bosch LLC, Corporate Research Davis, Ronald; Stanford University, Stanford Genome Technology Center Kavusi, Sam; Robert Bosch LLC, Corporate Research Ahmad, Habib; Robert Bosch LLC, Corporate Research



Journal Name

ARTICLE

## An electrochemical platform for localized pH control on demand

N. Fomina,<sup>a†</sup> C.A. Johnson,<sup>a†</sup> A. Maruniak,<sup>a</sup> S. Bahrapour,<sup>a</sup> C. Lang,<sup>a</sup> R.W. Davis,<sup>b</sup> S. Kavusi,<sup>a†\*</sup> and H. Ahmad<sup>a†\*</sup>

Received 00th January 20xx,  
Accepted 00th January 20xx

DOI: 10.1039/x0xx00000x

www.rsc.org/

Solution pH is a powerful tool for regulating many kinds of chemical activity, but is generally treated as a static property defined by a pre-selected buffer. Introducing dynamic control of pH in space, time, and magnitude can enable richer and more efficient chemistries, but is not feasible with traditional methods of titration or buffer exchange. Recent reports have featured electrochemical strategies for modifying bulk pH in constrained volumes, but only demonstrate switching between two preset values and omit spatial control entirely. Here, we use a combination of solution-borne quinones and galvanostatic excitation to enable quantitative control of pH environments that are highly localized to an electrode surface. We demonstrate highly reproducible acidification and alkalization with up to 0.1 pH/s ( $\pm 0.002$  pH/s) rate of change across the dynamic range of our pH sensor (pH 4.5 to 7.5) in buffered solutions. Using dynamic current control, we generate and sustain 3 distinct pH microenvironments simultaneously to within  $\pm 0.04$  pH for 13 minutes in a single solution, and we leverage these microenvironments to demonstrate spatially-resolved, pH-driven control of enzymatic activity. In addition to straightforward applications of spatio-temporal pH control (e.g. efficiently studying pH-dependencies of chemical interactions), the technique opens completely new avenues for implementing complex systems through dynamic control of enzyme activation, protein binding affinity, chemical reactivity, chemical release, molecular self-assembly, and many more pH-controlled processes.

### Introduction

pH is a fundamental property of aqueous solutions, and exerts a strong effect on many chemical processes. Perhaps its most interesting implications are in biological systems, where it is frequently leveraged as a tool to actively orchestrate sophisticated, multi-element regulation. Indeed, pH plays a crucial role in such diverse processes as intracellular sorting/targeting,<sup>1</sup> zymogen activation,<sup>2</sup> ATP synthesis,<sup>3</sup> cell migration,<sup>4</sup> signal transduction,<sup>5</sup> intercellular communication,<sup>6</sup> viral infection,<sup>7,8</sup> tumor growth and invasion,<sup>9,10</sup> and more.<sup>11,12</sup> The broad influence of pH in such systems derives from its critical role in determining the structure and function of proteins, in some cases to the extent that even very minor changes in pH can trigger dramatic differences in protein function.<sup>13</sup> A critical enabler for pH as a regulatory element is the cell's ability to sustain highly localized environments at precise pHs, and cells maintain a large apparatus of proteins dedicated to this task.<sup>11</sup>

Despite the evident potential of localized pH to realize complex systems, today's researchers only have access to relatively crude methods of achieving them; most pH transformations are performed using bulk buffers, which gives access to temporal – but not spatial – control. Conversely, approaches like gel matrices can provide spatial resolution, but not temporal. Recent progress in the microfluidics arena has yielded a few strategies for active, spatiotemporal pH control,<sup>14–18</sup> but these require flowing conditions to modify pH and are therefore best suited to immobilized targets.

One attractive method of dynamically modifying solution properties in static solutions is via electrochemical stimulus. This approach benefits from mature electronics that allow direct, quantitative control over the rate and magnitude of a reaction. Despite this potential for exerting precise regulation, the vast majority of electrochemical platforms are used for passive sensing rather than for active control.<sup>19</sup> Notable examples of the latter include: electrochemically-triggered release of biotin from gold electrodes via reduction and subsequent lactonization of a quinone tether<sup>20</sup> and electrochemical control of antibody immobilization at an electrode surface via redox of benzoquinones.<sup>21</sup> However, the potential for quantitative control in these applications is typically not exercised, as the systems are operated in a binary format.

<sup>a</sup> Robert Bosch LLC. Bosch Research & Technology Center, 4005 Miranda Ave., Palo Alto, CA 94304.

<sup>b</sup> Stanford University, Stanford, CA 94305.

\* Corresponding author: (phone) 650.320.1536; e-mail: habib.ahmad@us.bosch.com

† NF, CAJ, and HA contributed equally to the work.

‡ Current affiliation: Google Inc. 1600 Amphitheatre Pkwy, Mountain View, CA 94043

Electronic Supplementary Information (ESI) available: See DOI: 10.1039/x0xx00000x

This trend extends into demonstrations of active electrochemical control over solution pH. Most frequently, water electrolysis is employed to generate pulses of protons or hydronium ions to radically alter pH.<sup>15,22–27</sup> In other examples, protons are derived or consumed by additives in the solution, especially quinones.<sup>28,29</sup> However, to date, there has been little exploration of quantitative pH control using these methods. Willner and coworkers demonstrated a 3-dimensional layer of electroactive Au nanoparticles and thioanilines capable of modifying bulk pH in constrained volumes.<sup>30</sup> The extent of pH modulation was well-controlled by the thickness of this electroactive layer and the bulk solution volume, but the layer itself was activated in a binary mode to alternate between two preset pH values. Minero *et al.* recently employed a similar approach in microfluidics using polymerized quinones as a proton source. They extended the work to use free quinones in solution, but again employed a binary model to activating/reversing pH change while using buffer strength to broadly set the target pH.<sup>28</sup> Finally, Wang and coworkers utilized a serial, two-chambered electrolytic cell with a shared Pd thin foil. This allowed for rapid, hydrolysis-mediated pH swings via water electrolysis at moderate voltages; the resultant large swings in bulk pH were used to control DNA hybridization.<sup>31</sup>

In this paper we describe an electrochemical platform that enables quantitative control over pH at an electrode surface. We utilize a benign, quinone-based additive in conjunction with careful current shaping to regulate pH across a broad range, with tight spatio-temporal control and with unprecedented precision. We demonstrate reversible pH switching at a rate of 0.1 pH/s in the range between 4.5 and 7.5 in buffered solutions. This range is defined by the limits of our pH sensor, but is still sufficient to recreate many cellular environments. To this end, we demonstrate dynamic control over the activity of a pH-sensitive enzymatic process *in vitro*.

## Experimental

Enhanced Green Fluorescent Protein (eGFP) was purchased from BioVision Inc; pH-rodo and lysine fixable dextran-Fluorescein (MW 10,000) were purchased from Life Technologies. Dextranase was purchased from Sigma-Aldrich and dialyzed through a 1,000 molecular weight cut off (MWCO) membrane to remove buffer salts before use. All other chemical reagents and buffers were purchased from Sigma-Aldrich and used as received. Glass substrates with patterned ITO electrodes were purchased from Colorado Concept Coatings and functionalized by SCHOTT with their proprietary NEXTERION® H hydrogel coating.

NMR spectra were collected on a Varian 400. MALDI-TOF was collected on a Voyager-DE RP, using salicylic acid as a matrix. UV spectra were collected on a NanoDrop ND-1000. Proteins and dextran were spotted using a Scienion S3 spotter, were stored for at least 1 hour in a desiccator after spotting, and were tested within a week. Fluorescence data was acquired

with a Zeiss Axio Observer Z1. All electrochemical experiments were performed on a Metrohm Autolab PGSTAT101, using an ITO counter electrode and an Ag/AgCl reference. Multiplexed experiments were performed with the Metrohm MUX-MULTI4 module. Unless otherwise noted, electrochemical modulation was performed in 0.1x PBS buffer at pH 7.4 with 100 mM NaCl, 3.5 mM DMHQ, and 0.5 mM DMBQ. Bulk pH measurements were taken using a Metrohm 827 pH meter with a glass electrode.

pH readings were quantitated with the help of a custom image processing script using a 3-step process. First, an image was acquired such that several spots were visible on the working electrode (site of pH modulation) and an adjacent, non-stimulated electrode. The fluorescence intensity of individual spots was quantified using the entire spot area, and then adjusted on a per-spot basis to compensate for the local background. Second, the values from each electrode were averaged separately to yield single values for the working electrode and non-stimulated electrode; the working electrode value was then adjusted for signal loss on the non-stimulated electrode to account for photobleaching, yielding the final fluorescence intensity value. Third, this final value was expressed as a percentage of the fluorescence prior to modulation; the percentage was referenced against a standard curve generated with bulk pH buffers to derive the reported value.

### Synthesis of 2,5-dimethyl-1,4-hydroquinone:

Sodium dithionite (18.7 g, 107.3 mmol, 7.3 equiv) was dissolved in 20 mL H<sub>2</sub>O and loaded into a separatory funnel. Next, a solution of benzoquinone (2 g, 14.7 mmol, 1 equiv) in 75 mL diethyl ether was added. The biphasic mix was shaken vigorously for 30 minutes during which the organic layer changed color from orange to pale yellow. The organic phase was washed with brine, dried over MgSO<sub>4</sub>, and concentrated to yield a white solid (1.69 g, 83%).

<sup>1</sup>H NMR (DMSO-*d*<sub>6</sub>): 8.33 (s, 2H), 6.45 (s, 2H), 1.99 (s, 6H) ppm.

<sup>13</sup>C NMR (DMSO-*d*<sub>6</sub>): 147.38, 121.06, 116.75, 15.75 ppm.

### eGFP deactivation by BQ, MBQ, and DMBQ:

Solutions of 0.5 mM BQ, MBQ, and DMBQ were prepared separately using a base buffer of 0.1x PBS at pH 7.4 with 100 mM NaCl. eGFP was spotted onto a glass substrate bearing the NEXTERION® H coating; the glass was divided into discrete chambers using a silicone gasket and Teflon spacer. Four chambers were incubated with either a quinone solution or the base buffer for 30 min. Thereafter, the solutions were removed, the slide was washed with 0.1x PBS with 100 mM NaCl, and fluorescence images were recorded on a microscope. The quantitated fluorescence signal for each chamber was averaged from 12 individual GFP spots and reported as a percentage of that derived from the chamber containing base buffer (100%).

### Antibody modification with BQ and DMBQ:

Ab38C2 (3.75 mg/mL) was incubated in 0.1x PBS, pH 7.4, containing 5 mM BQ or DMBQ for 30 min. Small molecules were removed using Pierce Dye Removal Columns (22858). The number of molecules covalently bound to the antibody was calculated from the shift of *m/z* peak signal in MALDI-TOF as compared to an untreated sample.

#### Dextranase assay:

Dextran and eGFP were immobilized onto our platform via microspotting. For the bulk experiments, dextranase was reconstituted at 1  $\mu\text{g/mL}$  in citrate buffer (1 mM, 100 mM NaCl, pH 4.4 and pH 5.5) or PBS buffer (1 mM, 100 mM NaCl, pH 7.4). For electrochemical modulation, the enzyme was reconstituted at 1  $\mu\text{g/mL}$  in 0.1x PBS at pH 7.4 with 100 mM NaCl, 3.5 mM DMHQ, and 0.5 mM DMBQ. Control experiments utilized the same buffers, but without dextranase. A silicone gasket and Teflon spacer were used to divide the platform into multiple, identical chambers. Each solution was incubated in a separate chamber for 30 minutes, during which the quinone-bearing solutions were electrochemically modulated to maintain one of three fixed pHs for the entire duration. The pH achieved was reported by measuring eGFP as described earlier, while enzyme activity was assessed by comparing fluorescence images acquired before and after incubation; these images were acquired in 0.1x PBS, pH 7.4 buffer because the fluorescein dye has an appreciable pH response.

## Results and Discussion

### Platform description

Our platform is comprised of a standard lab glass slide (1"x3") which is patterned with an array of Indium Tin Oxide (ITO) electrodes. ITO is the most commonly used transparent conducting oxide material, and is advantageous in that it provides reasonable mobilities while preserving the optical transparency of the underlying glass substrate;<sup>32</sup> it is also amenable to many of the same chemical treatments commonly applied to standard glass (e.g. silane modification). For protein assays, we employ the Schott Nexterion H surface coating, a 3D thin-film polymer bearing reactive N-Hydroxysuccinimidyl ester (NHS) groups, to first enable protein immobilization and subsequently to minimize non-specific fouling. This allows the platform to function as a drop-in replacement for existing protein and cellular assays that employ optical readout. However, it is worth noting that, in several respects, ITO is far from an ideal electrode: in addition to a chemically unstable surface,<sup>33</sup> ITO suffers from very low electrochemical surface activity,<sup>34</sup> and consequently from inefficient electron transfer rates - especially with inner-sphere and Robin-Day Type M redox pairs,<sup>35</sup> including quinones. Therefore, in the absence of an optical requirement, the system may be implemented with more traditional metal or carbon electrodes to yield better performance.

pH modulation is effected through an electroactive agent added to the buffer, which incorporates chemically-reversible proton release/uptake upon electrochemical stimulation. This is preferable to the commonly-employed water electrolysis approach, as the high voltage required for the latter can

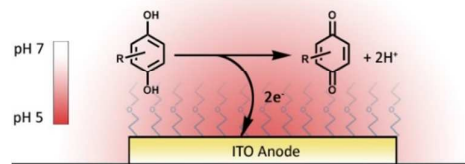


**Figure 1.** Schematic of localized pH modulation at an ITO electrode. Quinones diffuse through an anti-fouling polymer to the electrode surface where they undergo proton-coupled electron transfer; anodic currents liberate protons (shown), while cathodic currents consume protons. The resulting pH change is spatially constrained by the bulk buffer (here, PBS, pH 7), which continuously counteracts the perturbation. The balance between buffer capacity and electrode current primarily determines the surface pH and the spatial extent of pH modulation. Note that the schematic does not reflect the experimentally-derived dimensions of the pH gradient: while diffusion in the electrode plane is estimated, diffusion perpendicular to the electrode is not characterized in this work.

degrade ITO electrodes,<sup>36</sup> reduce the integrity of surface-bound layers,<sup>37</sup> and initiate undesirable side-reactions with protein/DNA analytes. Introducing the electroactive agent in solution rather than attaching it to the electrode surface confers three major advantages: firstly, pH modulation can be sustained for extended intervals due to continuous diffusion of the electroactive agent from the bulk; secondly, the electroactive agents are easier to synthesize and can be introduced only when pH modulation is necessary so as to minimize interference with assay components; thirdly, the substrate may be functionalized with standard surface treatments to enable continuity with prior work.

We utilize quinones as our electroactive agents due to their proton-coupled electron transfer, their relative chemical stability, and the substantial potential to tune their electrochemical and physical properties. Quinones are one of the most widely studied classes of electroactive molecules.<sup>38,39</sup> They are known to undergo inner-sphere electron transfer<sup>40</sup> in a  $2e^-/2H^+$  process,<sup>39</sup> and these two properties in concert form the basis for quantitative pH modulation.<sup>41,42</sup> Although inefficient electron transfer between ITO and quinones limits the scope of potentiostatic methods, a galvanostatic approach provides a quantitative measure of  $[H^+]$  produced/consumed at the electrode surface.

For simplicity, we focus on a conceptual description of the anodic reaction (Figure 1), but the reverse reaction occurs at the cathode such that the overall solution pH and hydroquinone/benzoquinone ratio is preserved despite the local gradients. As protons liberated at the anode surface diffuse away, they are rapidly neutralized by buffer molecules, keeping the zone of modulated pH localized. This state can be sustained for extended intervals because both the depleted

quinone and the depleted buffer species are continuously refreshed via passive diffusion from the bulk. Because the rate of buffer diffusion remains constant, the desired local pH can be stably maintained by balancing the rate of  $H^+$  generation against it. This implies that the quinone concentration and the stimulating current required for pH modulation are necessarily

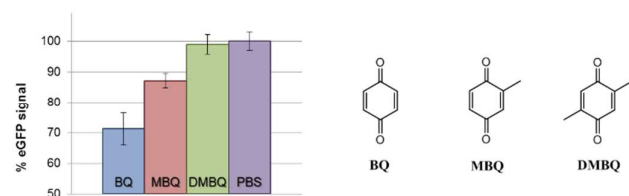


**Figure 2.** Benzoquinone toxicity towards eGFP protein is mitigated by increasing ring substitution, which diminishes its potential for Michael addition reactions. Such reactions compromise the structural integrity of proteins like eGFP, resulting in loss of function (here, fluorescence). Immobilized eGFP was incubated for 30 minutes with BQ, MBQ, and DMBQ separately (each at 0.5 mM in 1 mM PBS, pH 7.4). Quinone toxicity was quantified as the percentage of pre-incubation fluorescence that is preserved after treatment.

coupled with buffer strength to ensure a sufficient supply of protons under diffusion conditions. Note that buffer composition also plays an important role, as the buffering capacity of the bulk is maximal near each component's  $pK_a$ . Here, we utilize 0.1x PBS, 100mM NaCl, and a starting pH of 7.4 unless otherwise noted. We chose 1 mM buffer strength because it provides sufficient pH stability to the bulk solution, but at the same time places only moderate demands in terms of quinone concentration (here, 3.5mM hydroquinone and 0.5mM benzoquinone) and applied current. Chronopotentiometry experiments using typical excitation currents show a transition time ( $\tau$ ) > 120 minutes with this solution composition, giving an upper bound for maximum modulation time far in excess of the 15 minutes demonstrated in this work (Figure S1).

### Choice of electroactive molecules

The hydroquinone/benzoquinone redox pair has been used as a model system to produce proton gradients at electrode surfaces.<sup>28,43,44</sup> However, unsubstituted benzoquinones are known to undergo Michael addition reactions with nucleophiles, rendering them chemically incompatible with nucleophilic species, including many biomolecules<sup>45–47</sup>. Moreover, an ideal electroactive molecule must satisfy several additional constraints simultaneously: it must be water soluble in the millimolar range, it must be stable to auto-oxidation in ambient conditions, and it must be redox active within the potential windows of the working electrode (-0.7 V - +1.0 V vs. Ag/AgCl for ITO) and the biology.<sup>36</sup> The biological working window can vary significantly depending on the species under test, and may entirely preclude certain enzymes where quinones can serve as redox mediators. These notwithstanding, there is significant flexibility in the proposed system because the quinone core is amenable to ring modification, and because such modifications do not preclude

its proton-coupled electron transfer functionality. This allows the aforementioned requirements to be resolved synthetically.<sup>48–50</sup>

Due to the relatively substantial concentrations of quinone employed, low chemical reactivity is a primary concern. We tested a series of quinones to explore the relationship between biochemical compatibility and susceptibility to Michael addition. Unsubstituted benzoquinone (BQ) was compared with mono-substituted 2-methyl-1,4-benzoquinone (MBQ) and di-substituted 2,5-dimethyl-1,4-benzoquinone (DMBQ) using eGFP<sup>51</sup> as a compatibility marker. The fluorescence intensity of eGFP is tightly related to its structural integrity, such that loss of the former usually indicates a loss of tertiary structure.<sup>52</sup> Consequently, surface-bound eGFP was separately incubated with each of the three quinones for 30 minutes at room temperature. Fluorescence measurements preceding and following the incubation were used to track the percentage of fluorescence lost during exposure.

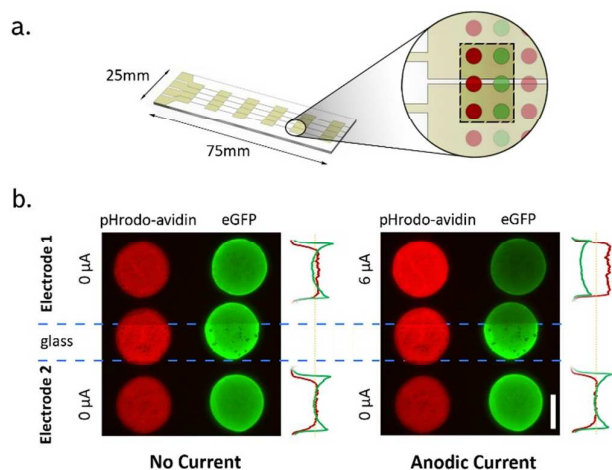
Figure 2 shows that adding steric bulk to sites susceptible to nucleophilic attack on the quinone correlated with sustained biomolecule activity. While the unsubstituted benzoquinone led to a 30% decrease in fluorescence, the mono-substituted quinone (MBQ) yielded 13% loss and the di-substituted quinone (DMBQ) resulted in only 1% loss of fluorescence. Although there is an increase in hydrophobicity concomitant with increasing ring substitution, our results suggest that the inactivation of eGFP stems from covalent modification via Michael addition rather than from hydrophobically-driven denaturation. To further substantiate this inactivation mechanism in the presence of biological nucleophiles, we incubated a murine antibody with a 200-fold molar excess of BQ and DMBQ for 30 minutes, and then analyzed the antibody via MALDI-TOF mass spectroscopy.<sup>53</sup> Mass shifts indicate an average of 15 binding events per antibody for BQ, whereas DMBQ exhibited substantially less (Figure S2).

Other compatibility requirements may be similarly tuned by careful selection of quinone substituents. Here, we found DMBQ to possess acceptable characteristics in each of the remaining categories: solubility is sufficient in PBS, the oxidation and reduction peaks were within the desired window (+0.88 V and -0.65 V vs. Ag/AgCl), respectively, Figure S3), and a solution of DMHQ in pH 7.4 was stable to auto-oxidation in air for several hours (Figure S4).

### Visualizing pH modulation

The electrochemical pH modulation technique detailed here creates a transient, highly localized, micron-scale pH gradient that cannot be measured by a typical glass electrode. Instead, we immobilize pH-sensitive fluorescent proteins at our electrode surface via microspotting onto an NHS-activated polymer surface. eGFP, and numerous variants thereof, exhibit strongly pH-dependent fluorescence, and are commonly employed to track the pH of intracellular

domains.<sup>54,55</sup> The technique is particularly well-suited to our application, as the protein-based pH sensor is expected to localize near the electrode with the same spatial distribution as other protein-based assays (as opposed to small organic or inorganic pH indicators). Thus, while the sensor is not informative of the gradient's full profile perpendicular to the electrode surface, its reported pH closely reflects the value that surface conjugated biomolecules are subjected to during normal operation. Moreover, immobilizing proteins is a facile

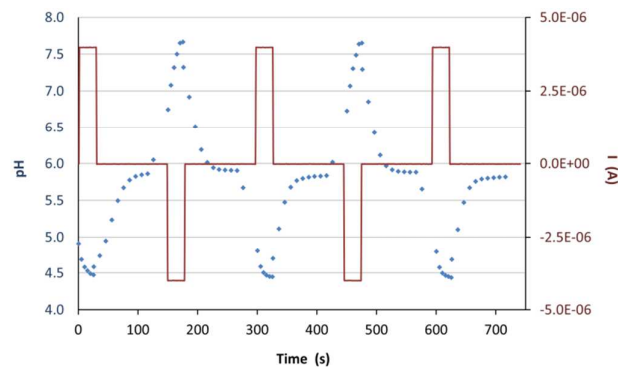


#### and efficient route

**Figure 3.** Electrochemical stimulation yields highly-localized changes in pH. a) Schematic of the pH modulation platform: a glass slide of standard dimensions bearing multiple ITO electrodes. The ITO electrode layout is flexible, and defines the morphology of potential pH microenvironments. Zoom shows protein spots at the boundary between two electrodes, as depicted in the micrograph below. b) pH sensitive proteins pHrodo-avidin and eGFP are microspotted across two ITO electrodes separated by a 100  $\mu\text{m}$  insulating glass gap, denoted by dotted blue lines. At left, the proteins are imaged under modulation buffer (3.5 mM MHQ, 0.5 mM MBQ, 0.1 M NaCl, 0.1x PBS, pH 7.4) without electrochemical stimulation. At right, anodic current is applied to Electrode 1 (6  $\mu\text{A}$ , 30 s), leading to localized acidification. The fluorescence intensity of proteins on Electrode 1 is modulated (pHrodo-avidin fluorescence increases below 7.4, eGFP fluorescence decreases), while those on Electrode 2 are unperturbed. The middle spots exhibit pH modulation with a sharp boundary corresponding to the ITO/glass transition; under these conditions, the pH microenvironment falls off within 20  $\mu\text{m}$  of the electrode edge. Quantitative traces at right are derived from vertical line profiles through the center of the spots. Scale bar (bottom right): 100  $\mu\text{m}$ .

to concentrate the sensor signal, enabling higher signal-to-noise ratio when compared with solvated sensors. As a proof of concept of localized pH modulation, we utilized eGFP and an additional probe: pHrodo avidin. The latter is an organic pH-sensitive dye conjugated to avidin protein in order to realize the benefits outlined above. The proteins were spotted onto our substrate in replicate such that they sampled the working electrode (Electrode 1), a control electrode that was not electrically stimulated (Electrode 2), and the insulating glass substrate between those electrodes, as shown in Figure 3. Both proteins' pH response was first characterized *in situ* using discrete buffered solutions at various known pHs to establish a calibration curve. In accordance with prior studies, eGFP shows a positive relationship between fluorescence and  $\text{pH}^{56,57}$ , while pHrodo avidin exhibits an inverse relationship<sup>58</sup>. The eGFP

calibration was also separately probed to confirm its stability throughout the course of a typical experiment (Figure S5). To demonstrate electrochemical pH modulation we substituted our standard quinone solution (0.1x PBS, pH 7.4) and applied an anodic current to Electrode 1, which is expected to decrease pH at the surface via oxidation of the hydroquinone. Figure 3b shows fluorescence images taken during such stimulation; both eGFP and pHrodo exhibit the expected response. Crucially, their fluorescence recovers to that of the



#### original, unstimulated

**Figure 4.** The chemically-reversible redox of quinones allows electrodes to establish both acidic and basic pH microenvironments with the same additive. A single electrode is bathed in modulation buffer (pH 5.8) and subjected to alternating, 30 s current pulses punctuated by 120 s rest periods while the surface pH is monitored in real-time. Anodic excitation acidifies the electrode surface, while cathodic excitation alkalinizes it. In the absence of active stimulation, the surface settles to the baseline pH as determined by the bulk buffer.

spots shortly after the current is stopped (evident in Figures 4-6) due to passive diffusion of the bulk buffer. This recovery, along with the enhanced fluorescence for pHrodo, demonstrate that the signal changes are specifically a response to local pH rather than an unintended side effect of an impinging voltage field, protein denaturation, or protein release from the surface. The experiment also demonstrates the high degree of pH localization that can be achieved with this modulation scheme: The middle spots in Figure 3b, which span the modulated electrode and the intermediate insulating glass substrate, are only modulated where they overlap the ITO electrode.

Quantitative measures of pH modulation in the remainder of this work were derived from similar microscope images, with a few changes. First, only eGFP was utilized as an indicator because it showed a more consistent response and higher signal than pHrodo (Figure S5). Second, the quantified signal was integrated over the entire area of each protein spot rather than using a simple line profile. A minimum of six spots were averaged per measurement, with standard deviations reported. Third, signal decay due to photobleaching was tracked by averaging intensities of eGFP spots on an adjacent, non-stimulated electrode (e.g. Electrode 2) and used to correct the signal from the working electrode. Following this correction, the remaining signal loss was calculated as a percentage of the signal at pH 7.4 and then translated into a

pH value by referencing against a pre-established standard curve (Figure S5a).

### Electrochemical pH modulation

Electrochemical systems may be driven via one of two fundamental excitation modes: potentiostatic or galvanostatic. The former approach is attractive because it allows precise control over which components of the system are electrochemically active, and because it can also provide some inherent level of feedback regulation in response to concentration gradients. However, potentiostatic methods are

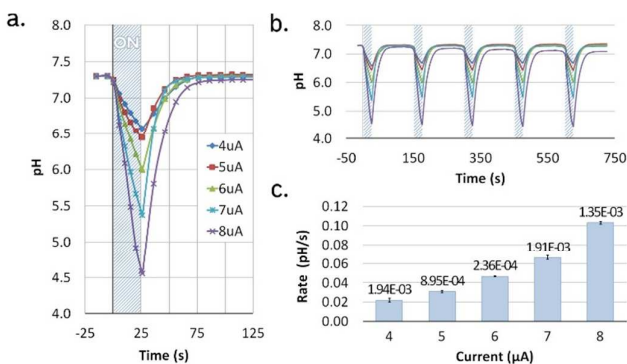


**Figure 5.** Galvanostatic excitation allows straightforward quantitative control over pH modulation. (a) An electrode is subjected to 25 s anodic current pulses at amplitudes from 4–8  $\mu\text{A}$  in 0.1x PBS, pH 7.4. The rate of pH modulation increases with current magnitude. (b) 5 sequential current pulses (denoted by shaded regions), with provision for relaxation after each, show good reproducibility of the modulation rate at each amplitude and no evidence of hysteresis. The 8  $\mu\text{A}$  trace exhibits some loss of signal with each cycle due to instability of the eGFP sensor below pH 5. (c) Modulation rate is calculated for each amplitude as the slope of the pH change during excitation. Standard deviation across the five cycles shown in (b) is quantified above each bar.

vulnerable to inter-substrate inconsistencies that yield unpredictable overpotentials, dynamic potential drifts, and uncompensated  $iR$  drops, making quantitative control a challenge. Conversely, galvanostatic excitation relinquishes electrochemical selectivity, but is impervious to shifting electrode impedances and presents a more intuitive approach to exerting quantitative control over a system. The selectivity problem can be mitigated by employing a quinone with sufficiently low  $E^0$ , and at concentrations where it will not be exhausted in standard operation (typically, equimolar with the buffer concentration). Here, we demonstrate the substantial control over local pH that is attainable through galvanostatic methods.

A key consequence of employing chemically-reversible quinone pairs as electroactive molecules is that simply changing the polarity of the applied current can yield acidic or alkaline modulation without need of additional species. Specifically, anodic currents liberate protons and thereby acidify the electrode environment, while cathodic currents consume protons to create an alkaline environment. Figure 4 demonstrates alternating cycles of acidic and basic microenvironments generated on the same electrode: cycles 1/3/5 were excited at +4.0  $\mu\text{A}$  for 30 s, while cycles 2/4 were

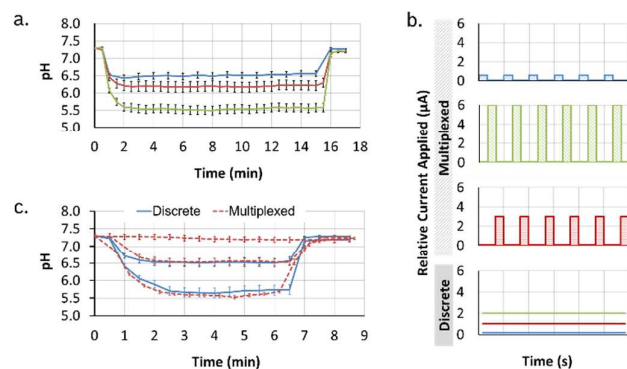
excited at -4.0  $\mu\text{A}$  for 30s. A 120 s rest period at open circuit potential allowed diffusion-driven recovery to the baseline after each excitation cycle, although this is by no means necessary. Indeed, direct application of the inverse current after an excitation cycle could be used to sharpen the return to baseline where required. Note that the pH of the bulk phosphate solution, which defines the baseline, was lowered to 5.8 to accommodate both cycles within the available dynamic range of eGFP (pH 4.5–7.5). Although the reproducibility of excitation cycles is quite good, there is a slight downward drift in the baseline pH which also manifests in the peak values attained during excitation. We ascribe this to a partial, but irreversible, loss of eGFP signal due to acid-induced denaturation rather than an actual change of bulk solution pH.<sup>52</sup> Similar loss of signal was observed in control experiments when eGFP was exposed to solutions with pH below 5 (Figure S5a).

Although eGFP limits the demonstrable range of pH modulation, it does not define the theoretical limits of our platform. The basic limit is defined by  $pK_{a2}$  of the quinone (for HQ: 11.84)<sup>39</sup>, beyond which its reduction is not accompanied by protonation. The converse limitation does not apply at the acidic end ( $pK_{a1}$  of BQ = -7)<sup>39</sup>, but a practical limitation may arise if the increasing oxidation potential exceeds the potential window of the biology or the substrate. Both limits are subject to tuning by modifying the electroactive molecule employed. These limits may be explored with alternative pH sensors, but in a biological context, even the demonstrated range is sufficient to simulate most known cellular environments<sup>58</sup>.

We explored the potential for a galvanostatic control scheme to produce quantitative modulation by cycling electrodes five times at each of five current magnitudes: 4, 5, 6, 7, and 8  $\mu\text{A}$  (Figure 5). Each cycle consisted of 30 s sustained anodic excitation followed by 120 s at rest at open circuit potential. As expected, the rate of pH modulation accelerates as the applied current is increased. We observed up to 0.1 pH/s, which roughly matches the rate of biological transients such as those found in the mitochondria (“mitoflashes”).<sup>59,60</sup> Crucially, this rate of change is highly reproducible – standard deviations are limited to  $< \pm 0.002$  pH/s over 5 cycles in all cases – and thereby enables more sophisticated implementations of pH control. For example, by applying a current waveform that continually balances the rate of proton generation with the inherent rate of buffer diffusion, a target pH may be sustained for extended intervals. Although this balance may be difficult to generate through other strategies, even highly complex waveforms are readily accessible with standard electronics. Figure 6a comprises readouts from three such waveforms; after an initial settling period of  $\sim 90$  s, stable pHs at 6.5, 6.2, and 5.5 are maintained for 13 min to within  $\pm 0.04$  pH. This stability is commensurate with the noise in our eGFP sensor, and an order of magnitude below the threshold required to trigger changes in even the most pH-sensitive biochemical systems.<sup>61</sup> We also characterized inter-substrate precision using galvanostatic control by reproducing the pH 6.2

excitation waveform on 22 additional electrodes spread across 4 additional substrates. The average pH recorded was  $6.21 \pm 0.098$  pH, while the pH stability of individual electrodes was maintained at  $\pm 0.046$  pH on average (Figure S6). We ascribe the variance among electrodes to inconsistent leakage currents and electrode surface inhomogeneity.

Electronically-driven pH control yields an additional, valuable benefit. Because the clock speed of our circuit far exceeds the ability of the chemical system to equilibrate, a single current source can be multiplexed across several electrodes. We demonstrate this concept by switching a single source across 3 electrodes in sequential, 100 ms bursts. The magnitude of each current burst varies with the electrode and with time, so



as to

**Figure 6.** Shaped excitation currents that balance the rates of  $H^+$  generation and buffer diffusion allow for fixed pH over extended intervals. (a) Stable pH microenvironments of 6.5, 6.2, and 5.5 are established on separate electrodes and maintained for 13 minutes to within  $\pm 0.04$  pH standard deviation. (b) Time multiplexed signals allow a single current source to drive multiple electrodes simultaneously as long as the total charge applied is preserved. Schematically, discrete signals of 0.1, 1, and 2  $\mu A$  are reproduced as repeated bursts of 0.3, 3, and 6  $\mu A$ , each applied for 1/3 of the excitation time. (c) a combination of (a) and (b) allows for multiple concurrent, stable pH microenvironments from a single current source with accuracy and stability commensurate with their discrete analogs (pH 6.5 and 5.5 demonstrated). Error bars in (a) and (c) represent standard deviation derived from 7 GFP spots on each of the modulated electrodes.

reproduce the waveforms for a constant pH of 7.4/6.5/5.5 on the first/second/third electrodes, respectively. However, since each electrode is only stimulated for one third of the time, the currents are scaled linearly by a factor of 3. Figure 6c illustrates the resulting pH environments, and shows that they closely match those arising from the corresponding discrete waveforms. These results further underscore the quantitative nature of galvanostatic control. The ability to simultaneously sustain multiple, localized pH environments without physical compartmentalization is a powerful, enabling technology that can help us begin to emulate the sophistication of biological systems.

### Modulation of enzymatic activity

As a practical demonstration of our platform, we sought to characterize the activity of an enzyme at multiple pHs. The pH response curve of an enzyme can provide insight into the chemistry of its active site as well as its broader function

within a cell. In addition to the convenience of replacing multiple discrete experiments with a single one, electrochemical modulation allows for a uniform buffer composition across the tested pH range. Enzyme activity is often sensitive to buffering species, which can yield discontinuity in data sets that employ different buffers to span large pH ranges.<sup>62</sup> More generally, the exquisite sensitivity of enzymes to their environment can help us to gauge how bio-orthogonal our modulation system is.

Dextranases are a highly-studied class of enzymes derived primarily from microbial sources. Here, we studied the pH dependence of a *Penicillium* endodextranase's activity against fluorescein-modified dextran. The latter was immobilized onto our platform and incubated for 30 minutes with enzyme-bearing solution at three fixed, electrochemically-regulated pHs. Dextranase activity was characterized by comparing the dextran's fluorescence intensity

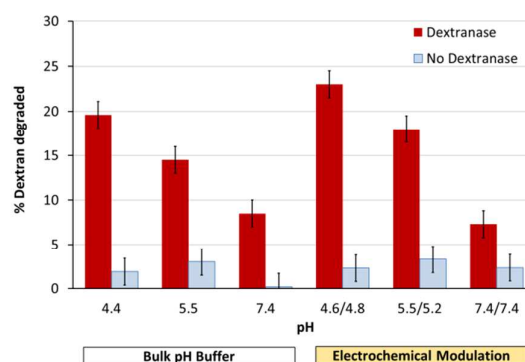


**Figure 7.** pH activity profiles for dextranase are similar when established via discrete buffers and via electrochemical modulation. Surface-immobilized, fluorescently-labelled dextran was exposed to dextranase-bearing solutions (1  $\mu g/mL$ , 30 minutes) with pH adjusted by bulk buffer or by local electrochemical modulation; loss of dextran from the surface is reported as a percentage of the original total. Control experiments performed with no dextranase (blue bars) confirm that dextran signal loss is enzymatically derived. Error bars represent standard deviation obtained from 6 dextran spots.

before and after the incubation. Figure 7 shows an inverse correlation between dextranase activity and pH. A similar trend was observed when the electrochemical modulation was substituted with discrete buffers at acidic pHs, and both results are in good agreement with existing literature on *Penicillium* dextranases, which indicates pH optimums of 4-6 for most variants.<sup>63</sup> The magnitude of activity change is likewise in accord with prior studies.<sup>64,65</sup> We also found minimal signal changes in the absence of dextranase, which confirms that the results are dictated by enzymatic hydrolysis rather than autodegradation, fluorophore inactivation by photobleaching, exposure to acidic pH, or interaction with electroactive molecules. Increased enzyme function under acidic pH (which is accompanied by elevated concentrations of oxidized quinone - a candidate for toxicity through Michael addition), indicates that such toxicity is not a significant factor here. Taken together with Figure 2, these results strongly suggest that our electrochemical pH modulation strategy is largely transparent to biochemical species, and thus well-suited for use in biological systems. Moreover, the ability to *electronically*

activate, deactivate, or dynamically tune the activity of enzymes with such broad applicability is, to our knowledge, unprecedented.

## Conclusions

We have demonstrated an electrochemical platform that enables on-demand pH control with micron-scale localization. By employing tailored quinones and a galvanostatic stimulus, we were able to acidify or alkalinize the solution at an electrode surface at highly reproducible rates up to 0.1 pH/s. Although we demonstrated pHs ranging from 4.5–7.5, these boundaries are defined by the dynamic range of our pH sensor, eGFP, rather than the fundamental potential of this approach. We also demonstrated that careful shaping of the excitation signal can sustain a desired pH microenvironment to within  $\pm 0.04$  pH for extended intervals. Crucially, the pH modulation components remained transparent, both figuratively and literally, to biological content on the platform. Given the strong biological inspiration for exploring localized pH, it is imperative that our solution is sufficiently bio-orthogonal to be useful in such systems. Similarly, the choice of ITO as an electrode material allows our platform to host a broad range of optical measurements common in biochemical systems.

The ability to dynamically generate localized pH microenvironments at a surface has many potential applications, including modulating antibody-antigen interactions, DNA hybridization, controlling enzymatic processes, studying protein aggregation/misfolding, cell manipulation, cell-free synthetic biology, controlled chemical release, electrostatic assembly of molecules on charged surfaces, fluorophore modulation, accelerating or inhibiting chemical reactions, and other processes that are fundamentally affected by pH. Biological systems have evolved to wring incredibly rich behaviours from such localized microenvironments, and serve as an example of the complexity that is at hand when pH is properly leveraged. The work presented here is an incremental step in our ability to likewise synthesize, process, and respond to complex chemical signals.

## Acknowledgements

We would like to thank Professor Neil Armstrong for many helpful discussions and suggestions with regards to using ITO as an electrode. We also thank Rajan Gangadharan for electrochemical characterization of electrode materials, Chaitanya Gupta for discussions on electrochemistry, Henrik Persson for discussions on surface chemistry, and Mehdi Javanmard for device fabrication and fruitful discussions.

## Notes and references

- O. A. Weisz, in *International Review of Cytology*, Elsevier, 2003, vol. 226, pp. 259–319.
- A. R. Khan and M. N. G. James, *Protein Sci.*, 2008, **7**, 815–836.

- P. Mitchell, *Nature*, 1961, **191**, 144–148.
- C. Martin, S. F. Pedersen, A. Schwab and C. Stock, *AJP Cell Physiol.*, 2011, **300**, C490–C495.
- M.-G. Ludwig, M. Vanek, D. Guerini, J. A. Gasser, C. E. Jones, U. Junker, H. Hofstetter, R. M. Wolf and K. Seuwen, *Nature*, 2003, **425**, 93–98.
- D. Gonzalez-Nieto, J. M. Gomez-Hernandez, B. Larrosa, C. Gutierrez, M. D. Munoz, I. Fasciani, J. O'Brien, A. Zappala, F. Czirata and L. C. Barrio, *Proc. Natl. Acad. Sci.*, 2008, **105**, 17169–17174.
- P. A. Bullough, F. M. Hughson, J. J. Skehel and D. C. Wiley, *Nature*, 1994, **371**, 37–43.
- L. S. Ehrlich, T. Liu, S. Scarlata, B. Chu and C. A. Carter, *Biophys. J.*, 2001, **81**, 586–594.
- R. A. Gatenby and R. J. Gillies, *Nat. Rev. Cancer*, 2004, **4**, 891–899.
- R. Martínez-Zaguilán, E. A. Seftor, R. E. B. Seftor, Y.-W. Chu, R. J. Gillies and M. J. C. Hendrix, *Clin. Exp. Metastasis*, 1996, **14**, 176–186.
- J. R. Casey, S. Grinstein and J. Orlowski, *Nat. Rev. Mol. Cell Biol.*, 2010, **11**, 50–61.
- J. Srivastava, D. L. Barber and M. P. Jacobson, *Physiology*, 2007, **22**, 30–39.
- S. T. Whitten, B. G.-M. E and V. J. Hilser, *Proc. Natl. Acad. Sci. U. S. A.*, 2005, **102**, 4282–4287.
- A. Atwe, A. Gupta, R. Kant, M. Das, I. Sharma and S. Bhattacharya, *Microsyst. Technol.*, 2014, **20**, 1373–1381.
- H. Zhou, G. Li and S. Yao, *Lab. Chip*, 2014, **14**, 1917–1922.
- D. Welch and J. B. Christen, *Lab. Chip*, 2014, **14**, 1191–1197.
- C. R. Cabrera, B. Finlayson and P. Yager, *Anal. Chem.*, 2001, **73**, 658–666.
- S. Böhm, W. Olthuis and P. Bergveld, *Sens. Actuators B Chem.*, 1998, **47**, 48–53.
- R. M. Penner, *Nat. Chem.*, 2010, **2**, 251–252.
- C. D. Hodneland and M. Mrksich, *J. Am. Chem. Soc.*, 2000, **122**, 4235–4236.
- Y. L. Bunimovich, G. Ge, K. C. Beverly, R. S. Ries, L. Hood and J. R. Heath, *Langmuir*, 2004, **20**, 10630–10638.
- E. Brod, S. Nimri, B. Turner and U. Sivan, *Sens. Actuators B Chem.*, 2008, **128**, 560–565.
- P. Kauffman, E. Fu, B. Lutz and P. Yager, *Lab. Chip*, 2010, **10**, 2614.
- S. O. Krabbenborg, C. Nicosia, P. Chen and J. Huskens, *Nat. Commun.*, 2013, **4**, 1667.
- K. Morimoto, M. Toya, J. Fukuda and H. Suzuki, *Anal. Chem.*, 2008, **80**, 905–914.
- J. Suzurikawa, M. Nakao, R. Kanzaki and H. Takahashi, *Sens. Actuators B Chem.*, 2010, **149**, 205–211.
- E. L. May and A. C. Hillier, *Anal. Chem.*, 2005, **77**, 6487–6493.
- G. A. S. Minero, P. F. Wagler, A. A. Oughli and J. S. McCaskill, *RSC Adv*, 2015, **5**, 27313–27325.
- D. Kohlheyer, J. C. T. Eijkel, S. Schlautmann, A. van den Berg and R. B. M. Schasfoort, *Anal. Chem.*, 2008, **80**, 4111–4118.
- M. Frasconi, R. Tel-Vered, J. Elbaz and I. Willner, *J. Am. Chem. Soc.*, 2010, **132**, 2029–2036.
- Y.-C. Wang, C.-B. Lin, J.-J. Su, Y.-M. Ru, Q. Wu, Z.-B. Chen, B.-W. Mao and Z.-W. Tian, *Anal. Chem.*, 2011, **83**, 4930–4935.
- K. Ellmer, *Nat. Photonics*, 2012, **6**, 809–817.
- M. Brumbach, P. A. Veneman, F. S. Marrikar, T. Schulmeyer, A. Simmonds, W. Xia, P. Lee and N. R. Armstrong, *Langmuir*, 2007, **23**, 11089–11099.
- F. S. Marrikar, M. Brumbach, D. H. Evans, A. Lebrón-Paler, J. E. Pemberton, R. J. Wysocki and N. R. Armstrong, *Langmuir*, 2007, **23**, 1530–1542.
- S. V. Rosokha and J. K. Kochi, *J. Am. Chem. Soc.*, 2007, **129**, 3683–3697.
- M. Senthilkumar, J. Mathiyarasu, J. Joseph, K. L. N. Phani and V. Yegnaraman, *Mater. Chem. Phys.*, 2008, **108**, 403–407.

- 37 C. S. Tang, P. Schmutz, S. Petronis, M. Textor, B. Keller and J. Vörös, *Biotechnol. Bioeng.*, 2005, **91**, 285–295.
- 38 P. S. Guin, S. Das and P. C. Mandal, *Int. J. Electrochem.*, 2011, **2011**, 1–22.
- 39 M. Quan, D. Sanchez, M. F. Wasylkiw and D. K. Smith, *J. Am. Chem. Soc.*, 2007, **129**, 12847–12856.
- 40 S. H. DuVall and R. L. McCreery, *J. Am. Chem. Soc.*, 2000, **122**, 6759–6764.
- 41 C. Batchelor-McAuley, B. R. Kozub, D. Menshkykau and R. G. Compton, *J. Phys. Chem. C*, 2011, **115**, 714–718.
- 42 E. B. Carneiro-Neto, M. C. Lopes and E. C. Pereira, *J. Electroanal. Chem.*, 2015, **765**, 92–99.
- 43 N. C. Rudd, S. Cannan, E. Bitziou, I. Ciani, A. L. Whitworth and P. R. Unwin, *Anal. Chem.*, 2005, **77**, 6205–6217.
- 44 S. Fiedler, R. Hagedorn, T. Schnelle, E. Richter, B. Wagner and G. Fuhr, *Anal. Chem.*, 1995, **67**, 820–828.
- 45 J. L. Bolton, M. A. Trush, T. M. Penning, G. Dryhurst and T. J. Monks, *Chem. Res. Toxicol.*, 2000, **13**, 135–160.
- 46 X. Wang, B. Thomas, R. Sachdeva, L. Arterburn, L. Frye, P. G. Hatcher, D. G. Cornwell and J. Ma, *Proc. Natl. Acad. Sci.*, 2006, **103**, 3604–3609.
- 47 A. G. Siraki, *Toxicol. Sci.*, 2004, **81**, 148–159.
- 48 M. L. Fultz and R. A. Durst, *Anal. Chim. Acta*, 1982, **140**, 1–18.
- 49 M. G. Evans and J. De Heer, *Q. Rev. Chem. Soc.*, 1950, **4**, 94.
- 50 M. Namazian and H. A. Almodarresieh, *J. Mol. Struct. THEOCHEM*, 2004, **686**, 97–102.
- 51 B. P. Cormack, R. H. Valdivia and S. Falkow, *Gene*, 1996, **173**, 33–38.
- 52 M. Kneen, J. Farinas, Y. Li and A. S. Verkman, *Biophys. J.*, 1998, **74**, 1591–1599.
- 53 R. Weinstein, P. S. Baran and D. Shabat, *Bioconjug. Chem.*, 2009, **20**, 1783–1791.
- 54 M. Benčina, *Sensors*, 2013, **13**, 16736–16758.
- 55 S. G. Olenych, N. S. Claxton, G. K. Ottenberg and M. W. Davidson, in *Current Protocols in Cell Biology*, eds. J. S. Bonifacino, M. Dasso, J. B. Harford, J. Lippincott-Schwartz and K. M. Yamada, John Wiley & Sons, Inc., Hoboken, NJ, USA, 2007.
- 56 J. Llopis, J. M. McCaffery, A. Miyawaki, M. G. Farquhar and R. Y. Tsien, *Proc. Natl. Acad. Sci.*, 1998, **95**, 6803–6808.
- 57 G. H. Patterson, S. M. Knobel, W. D. Sharif, S. R. Kain and D. W. Piston, *Biophys. J.*, 1997, **73**, 2782–2790.
- 58 J. Han and K. Burgess, *Chem. Rev.*, 2010, **110**, 2709–2728.
- 59 J. Santo-Domingo, M. Giacomello, D. Poburko, L. Scorrano and N. Demaurex, *EMBO J.*, 2013, **32**, 1927–1940.
- 60 M. Schwarzländer, S. Wagner, Y. G. Ermakova, V. V. Belousov, R. Radi, J. S. Beckman, G. R. Buettner, N. Demaurex, M. R. Duchon, H. J. Forman, M. D. Fricker, D. Gems, A. P. Halestrap, B. Halliwell, U. Jakob, I. G. Johnston, N. S. Jones, D. C. Logan, B. Morgan, F. L. Müller, D. G. Nicholls, S. J. Remington, P. T. Schumacker, C. C. Winterbourn, L. J. Sweetlove, A. J. Meyer, T. P. Dick and M. P. Murphy, *Nature*, 2014, **514**, E12–E14.
- 61 B. Trivedi and W. H. Danforth, *J. Biol. Chem.*, 1966, **241**, 4110–4112.
- 62 S. O. Ugwu and S. P. Apte, *Pharm. Technol.*, 2004, **28**, 86–109.
- 63 E. R. Jiménez, *Sugar Tech*, 2009, **11**, 124–134.
- 64 Madhu and K. A. Prabhu, *Enzyme Microb. Technol.*, 1984, **6**, 217–220.
- 65 D. Koenig and D. Day, *Eur. J. Biochem.*, 1989, **183**, 161–167.